DOI: 10.1002/ejic.201100276

Solution Chemistry Synthesis of Intermetallic Gold–Lithium Nanoparticles

James F. Bondi[a] and Raymond E. Schaak*[a,b]

Dedicated to Professor John D. Corbett on the occasion of his 85th birthday

Keywords: Gold / Lithium / Nanoparticles / Intermetallic phases

Colloidal nanoparticles of a prototype polar intermetallic compound, Au_3Li, were synthesized by reacting Au nanoparticle seeds with *n*-butyllithium. X-ray and electron diffraction data are consistent with the $L1_2$ (Cu_3Au) structure type expected for Au_3Li. Composition analysis indicates a stoichiometry of approximately $Au_3Li_{0.7}$, which is within the reported composition range of the Au_3Li phase. The Au_3Li nanoparticles decompose in water to regenerate Au. The successful synthesis of Au_3Li as colloidal nanoparticles demonstrates that polar intermetallic compounds containing highly electropositive elements are accessible by using low-temperature solution chemistry routes and that they are also amenable to nanostructuring.

Introduction

Polar intermetallic compounds combine electronegative and electropositive elements to form phases that contain polycationic or polyanionic metallic clusters or networks.[1] Au-based polar intermetallics are particularly interesting because of the impact that relativistic effects have on the structures and phases that form.[2] Many examples of polar intermetallic compounds containing gold are known, including the ternary phases $BaAu_2In_2$,[3] $SrAuIn_3$,[4] Rb_2Au_3Tl,[5] KAu_4In_2,[6] and $Ca_4Au_{10}In_3$.[7] Binary intermetallic compounds of gold with alkali metals are also interesting. These alkali aurides exhibit complex phase relations and structures that are stabilized by relativistic bonding interactions, which are dependent upon the electronegativity of the alkali metal.[8,9]

Most polar intermetallic compounds are synthesized by the direct combination of the constituent elements at elevated temperatures.[10] The desire for exploratory investigations that facilitate the discovery of new polar intermetallic compounds,[1] coupled with the desire to access polar intermetallic compounds in nanoparticle form for their potential use as highly active catalysts,[11] motivates an alternative synthetic regime for accessing these materials. Here, we report a low-temperature solution chemistry method for the synthesis of a prototype polar intermetallic compound, Au_3Li (Figure 1). Although it has not been extensively studied, Au_3Li is a known phase that has been reported to adopt the $L1_2$ (Cu_3Au) structure type.[12,13] This corresponds to the α_1 phase on the Au–Li phase diagram, which forms over a relatively wide composition window.[12] To synthesize nanoparticles of Au_3Li, colloidal Au nanoparticles are synthesized first, and these Au nanoparticle seeds are converted to Au_3Li upon reaction with *n*-butyllithium (*n*BuLi). To the best of our knowledge, this is the first report describing colloidal nanoparticles of a polar intermetallic compound containing a highly electropositive element such as Li. This synthetic strategy has the potential

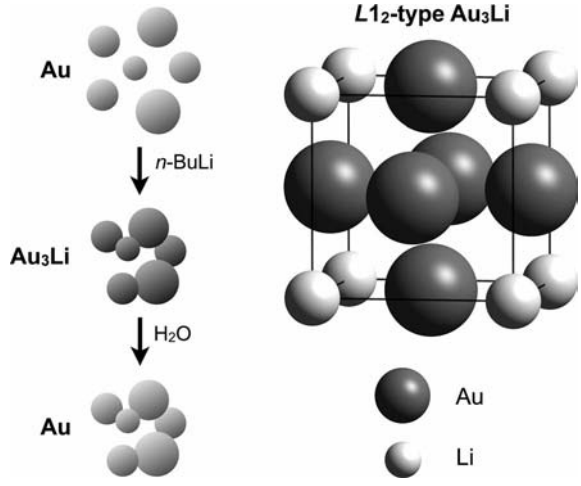

Figure 1. (Left) Scheme showing the formation of Au_3Li by reaction of preformed Au nanoparticles with *n*BuLi, followed by decomposition to regenerate Au when treated with water. (Right) $L1_2$ crystal structure of Au_3Li.

[a] Department of Chemistry, The Pennsylvania State University, University Park, Pennsylvania 16802, USA
E-mail: schaak@chem.psu.edu
[b] Materials Research Institute, The Pennsylvania State University,
University Park, Pennsylvania 16802, USA

to be general, which could lead to the synthesis of other known and new polar intermetallic compounds as colloidal nanoparticles for applications that include catalysis and lithium batteries.[11,14]

Results and Discussion

In a typical synthesis (described in detail in the Experimental Section), Au nanoparticles are formed first by the reduction of $HAuCl_4 \cdot 3H_2O$ with oleylamine in diphenyl ether at 80 °C (Figure 1). The powder X-ray diffraction (XRD) pattern in Figure 2 confirms the formation of nanocrystalline Au with an average grain size of 6.1 nm, as estimated by using the Scherrer equation. The transmission electron microscopy (TEM) image of these Au seeds, presented in the inset to Figure 2, shows spherical particles with an average diameter of 6.2 ± 1.9 nm. This is consistent with the XRD data and indicates that the particles are, on average, single-domain crystals. The selected area electron diffraction (SAED) pattern is also consistent with the formation of face centered cubic (fcc) Au.

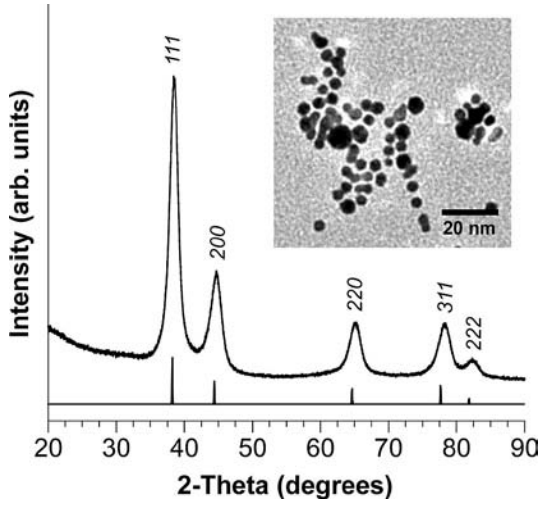

Figure 2. Powder XRD data for the Au nanoparticle seeds formed at 80 °C. A reference pattern for Au is shown below, and the indexing corresponds to fcc Au. A TEM image of the Au nanoparticle seeds is shown in the inset.

The Au seed particles are then reacted with a solution of *n*BuLi in diphenyl ether and heated to 248 °C under rigorously air-free conditions. This synthetic procedure is very closely related to that used to form $L1_2$-type Au_3Fe, Au_3Co, and Au_3Ni,[15,16] except that no 3d transition metal reagents are present in this case. Figure 3 shows the XRD pattern for the Au_3Li nanoparticles, which clearly shows the superlattice peaks expected for the $L1_2$ structure type. The relative intensities also match well with those expected for $L1_2$-type Au_3Li. The refined lattice constant for Au_3Li is a = 3.994(6) Å, which is smaller than that of Au (a_{Au} = 4.078 Å) and matches more closely with that expected for Au_3Li (a_{Au_3Li} = 3.973 Å).[12] From Vegard's law, the composition is estimated to be $Au_3Li_{0.8}$, on the basis of Au and stoichiometric Au_3Li as end members.

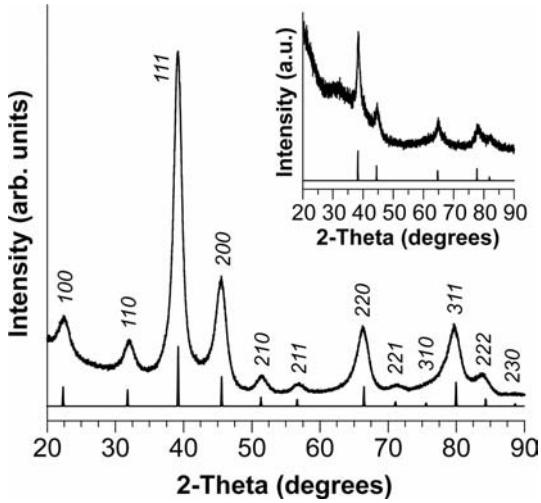

Figure 3. Powder XRD data for intermetallic Au_3Li nanoparticles, along with an $L1_2$-type Au_3Li reference pattern for comparison. Powder XRD data of the product after the reaction of Au_3Li with water, shown in the inset, corresponds to fcc Au.

Figure 4a shows a representative TEM image of the Au_3Li nanoparticles, which are agglomerated but generally retain the spherical morphology of the Au seeds. The average diameter of the primary particles that comprise the aggregates is 9.1 ± 2.4 nm, which is larger than the size of the Au nanoparticle seeds. The size increase upon reaction with *n*BuLi to form Au_3Li is attributed primarily to the higher reaction temperature, which facilitates coalescence and growth relative to the lower temperature used to synthesize the Au seeds. High-resolution TEM (HRTEM) images of Au_3Li particles show lattice fringes corresponding to the *100* (d = 4.0 Å), *110* (d = 2.8 Å), and *111* (d = 2.3 Å) planes (Figure 4b), which is consistent with the formation of $L1_2$-type Au_3Li. The SAED pattern in Figure 4a is also consistent with the $L1_2$ structure of the nanoparticles, the *100* and *110* superlattice reflections being clearly evident.

Composition analysis of the Au_3Li nanoparticles by energy dispersive spectroscopy (EDS) shows only Cu (from the TEM grid) and Au, because Li cannot be detected by EDS (Figure 4c). (Carbon is also observed by EDS, and this is attributed to the TEM grid and oleylamine.) While X-ray photoelectron spectroscopy (XPS) and electron energy loss spectroscopy (EELS) can both detect Li and were used to characterize the Au_3Li nanoparticles, the results are inconclusive because the primary peaks for the Au 5p3/2 and the Li 1s core level region overlap for both of these techniques.[17,18] Instead, inductively coupled plasma mass spectrometry (ICP-MS) was used to confirm the presence of Li in the Au_3Li nanoparticles. Assuming that the entire mass of the sample used for ICP-MS analysis corresponded to Au_3Li, the lithium content was found to be approximately 68% of the value expected for stoichiometric Au_3Li, which indicates an approximate composition of $Au_3Li_{0.7}$. This value represents a lower limit, however, because the presence of surface ligands on the Au_3Li nanoparticles

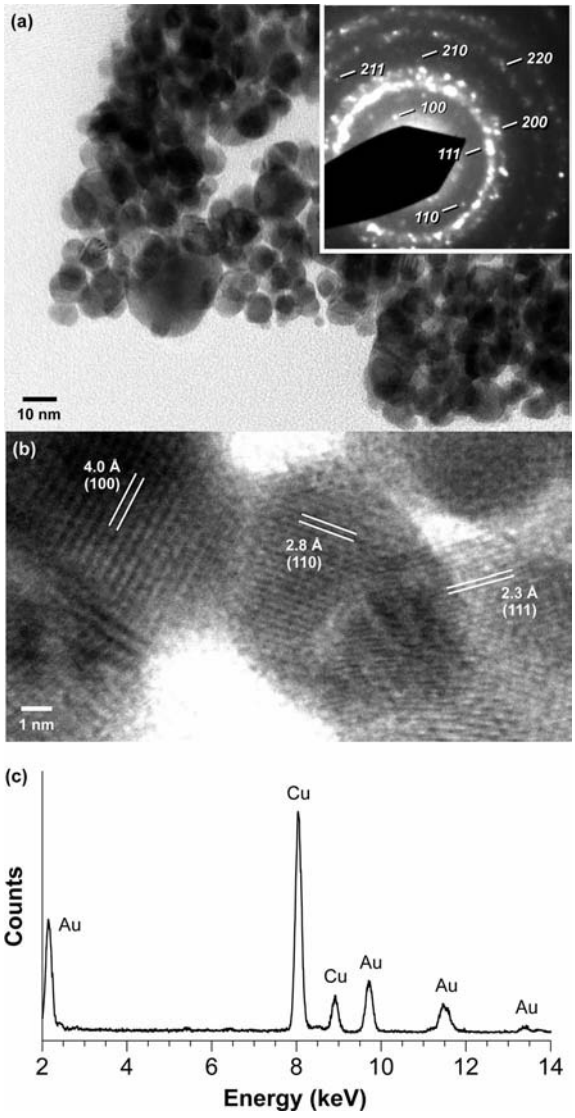

Figure 4. (a) Representative TEM image of the Au_3Li nanoparticles, with the corresponding indexed SAED pattern shown in the inset; (b) HRTEM image showing lattice fringes corresponding to the *100* (d = 4.0 Å), *110* (d = 2.8 Å), and *111* (d = 2.3 Å) planes of Au_3Li; (c) EDS data for the Au_3Li particles, showing only Cu (from the TEM grid) and Au.

makes the mass of the Au_3Li component smaller than the total mass of the entire ICP-MS sample. However, thermogravimetric analysis (TGA) indicates an average mass loss of only approximately 2% up to 400 °C, which implies that an average composition of $Au_3Li_{0.7}$ is a realistic estimate. This sub-stoichiometric composition is within the reported range of phase stability for Au_3Li[12] and is also consistent with the estimated composition of $Au_3Li_{0.8}$ based on a Vegard's law analysis of the lattice constants.

The Au_3Li nanoparticles are air-stable in powder form, with no significant change observed by XRD over a time period of 3 months. However, when dispersed in water and stirred for 1 h at room temperature, the Li is removed, and Au nanoparticles are regenerated. The XRD pattern for the product after reaction with water, shown in the inset to Figure 3, is consistent with fcc Au and has no evidence of the $L1_2$ superlattice peaks. ICP-MS analysis of the supernatant shows the presence of Li at a level that is consistent with the amount that is incorporated into the $Au_3Li_{0.7}$ phase. The fact that Au_3Li decomposes in water is consistent with its polar intermetallic nature, and suggests that this material could undergo facile Li insertion and extraction.

The formation of Au_3Li by a synthetic protocol that is closely related to that used to form the $L1_2$-type Au_3M (M = Fe, Co, Ni) intermetallics is also interesting.[15,16] EDS analysis, including detailed refinement of the EDS data,[19] indicated substoichiometric Fe, Co, and Ni in the Au_3M nanoparticles, suggesting a true composition of Au_3M_{1-x}.[16] The fact that Au_3Li forms under similar conditions implies that Li may be incorporated in the Au_3M_{1-x} nanoparticles, perhaps existing as $Au_3M_{1-x}Li_x$.

Conclusions

We have shown that colloidal Au nanoparticles can serve as a template for lithium insertion by reaction with *n*BuLi to form $L1_2$-type Au_3Li. This represents a solution chemistry route to a prototype polar intermetallic compound containing a highly electropositive element. As a complement to traditional synthetic routes, this alternative low-temperature synthetic strategy may lead to the synthesis and discovery of other polar intermetallic compounds, including other alkali metal systems with use of reagents such as sodium naphthalide. The successful synthesis of a polar intermetallic compound as colloidal nanoparticles also demonstrates that this rich class of solid-state materials is amenable to nanostructuring by using solution synthesis techniques.

Experimental Section

General: All reactants were prepared in an Ar-atmosphere glove box, and the reactions were carried out under ultra-high-purity (UHP) Ar with standard Schlenk techniques. Oleylamine (70% technical grade) was purchased from Sigma Aldrich, and $HAuCl_4 \cdot 3H_2O$ (99.99%), *n*-butyllithium (*n*BuLi, 2.5 M in hexane), and diphenyl ether (99% reagent grade) were purchased from Alfa Aesar. As-received $HAuCl_4 \cdot 3H_2O$ and *n*BuLi were transferred to and stored in an Ar-atmosphere glove box. Diphenyl ether and oleylamine were dried by heating to 110 °C for 1 h under vacuum to remove any excess water and transferred into the glove box by using a freeze-thaw degassing method, and stored with 3 Å molecular sieves. Extreme caution must always be taken when using *n*BuLi because of its air-sensitive nature. XRD data were collected with a Bruker Advance D8 X-ray diffractometer using Cu-K_α radiation. Lattice constants were refined with the Chekcell program. TEM images, EDS spectra, and SAED patterns were collected with a JEOL-2010 LaB_6 microscope operating at 200 kV with an EDAX solid state detector. Samples for TEM, EDS, and SAED were prepared by redispersing the nanoparticles in hexanes and drop coating onto a carbon-coated copper grid. ICP-MS data were collected with a Thermo Fisher Scientific X Series 2 with collision cell technology. TGA was performed with a TA Instruments SDT Q600

instrument with alumina crucibles, 5–10 mg of sample, and a heating rate of 2 °C per min under Ar.

Synthesis of Au_3Li Nanoparticles: Inside an Ar-filled glove box, $HAuCl_4 \cdot 3H_2O$ (50 mg) was placed in a 50 mL 3-neck flask. Next, diphenyl ether (10 mL) and oleylamine (250 μL) were added to the 3-neck flask. The 3-neck flask was sealed by using a condenser with an airflow adapter on top, a thermometer adapter with a mercury thermometer, and a 14/20 rubber septum. Also in the glove box, diphenyl ether (5 mL) and *n*BuLi (2.0 mL, 2.5 M in hexane) were added to a 50 mL Schlenk flask, which was sealed with a rubber septum. Both the sealed 3-neck flask and the sealed Schlenk flask were removed from the glove box. The 3-neck apparatus was sonicated for ca. 30 min until all of the metal salt was dissolved. At the same time, the Schlenk flask was connected to a Schlenk line under ultra-high-purity Ar, and the hexanes were removed from the *n*BuLi solution by vacuum for 30 min in order to prevent dangerous overpressure during injection. After that, the 3-neck flask was attached to the Schlenk line, flushed, and evacuated with Ar three times. The 3-neck flask was then filled with Ar, and the reaction was performed under an Ar blanket. The 3-neck flask was heated to 80 °C over the course of 40 min and stirred for an additional 20 min, at which point the *n*BuLi solution was released from vacuum, filled with Ar, and injected into the 3-neck flask with a metal syringe. Finally, the solution mixture in the 3-neck flask was heated to reflux at 248 °C over 75 min, after which the heating source was turned off and the reaction was allowed to cool to room temperature. Work-ups were performed in air, and ethanol was added to the reaction to quench any unreacted *n*BuLi.

Acknowledgments

This work was supported by the U. S. Department of Energy (DE-FG02-08ER46483). Electron microscopy was performed at the Penn State Materials Research Institute. The authors acknowledge use of facilities at the Pennsylvania State University site of the National Science Foundation NNIN (National Nanotechnology Infrastructure Network), and thank Waleska Castro of the Materials Research Institute for acquisition of the ICP-MS data.

[1] J. D. Corbett, *Inorg. Chem.* **2010**, *49*, 13–28.
[2] P. Pyykkö, *Angew. Chem.* **2002**, *114*, 3723; *Angew. Chem. Int. Ed.* **2002**, *41*, 3573–3578.
[3] U. Zachwieja, *Z. Anorg. Allg. Chem.* **1998**, *624*, 1443–1446.
[4] S. Liu, J. D. Corbett, *Inorg. Chem.* **2004**, *43*, 4988–4993.
[5] B. Li, S.-J. Kim, G. J. Miller, J. D. Corbett, *Inorg. Chem.* **2009**, *48*, 6573–6583.
[6] B. Li, J. D. Corbett, *J. Am. Chem. Soc.* **2006**, *128*, 12392–12393.
[7] Q. Lin, J. D. Corbett, *Inorg. Chem.* **2007**, *46*, 8722–8727.
[8] P. Schwerdtfeger, M. Dolg, W. H. Eugen Schwarz, G. A. Bowmaker, P. D. W. Boyd, *J. Chem. Phys.* **1989**, *91*, 1762–1774.
[9] R. E. Watson, M. Weinert, *Phys. Rev. B* **1994**, *49*, 7148–7154.
[10] J. D. Corbett, E. Garcia, A. M. Guloy, W.-M. Hurng, Y.-U. Kwon, E. A. Leon-Escamilla, *Chem. Mater.* **1998**, *10*, 2824–2836.
[11] V. Hlukhyy, F. Raif, P. Claus, T. F. Fässler, *Chem. Eur. J.* **2008**, *14*, 3737–3744.
[12] A. D. Pelton, *Bull. Alloy Phase Diagrams* **1986**, *7*, 228–231.
[13] G. Kienast, J. Verma, *Z. Anorg. Allg. Chem.* **1961**, *310*, 143–169.
[14] S. C. Mui, P. E. Trapa, B. Huang, P. P. Soo, M. I. Lozow, T. C. Wang, R. E. Cohen, A. N. Mansour, S. Mukerjee, A. M. Mayes, D. R. Sadoway, *J. Electrochem. Soc.* **2002**, *149*, A1610–A1615.
[15] Y. Vasquez, Z. Luo, R. E. Schaak, *J. Am. Chem. Soc.* **2008**, *130*, 11866–11867.
[16] J. F. Bondi, R. Misra, X. Ke, I. T. Sines, P. Schiffer, R. E. Schaak, *Chem. Mater.* **2010**, *22*, 3988–3994.
[17] M. Cardona, L. Ley (Eds.), *Photoemission in Solids I: General Principles*, Springer-Verlag, Berlin, **1978**.
[18] J. C. Fuggle, N. Mårtensson, *J. Electron Spectrosc. Relat. Phenom.* **1980**, *21*, 275–281.
[19] Z. Luo, Y. Vasquez, J. F. Bondi, R. E. Schaak, *Ultramicroscopy* **2011**, DOI: 10.1016/j.ultramic.2011.04.003.

Received: March 19, 2011
Published Online: May 24, 2011

